Toward Transition Modeling in a Hypersonic Boundary Layer at Flight Conditions

Pedro Paredes,* Balaji Venkatachari,†
National Institute of Aerospace, Hampton, VA 23666, USA

Meelan M. Choudhari,‡ Fei Li,§ Chau-Lyan Chang,¶
NASA Langley Research Center, Hampton, VA 23681, USA

Muhammad I. Zafar,‖ Heng Xiao**
Virginia Tech, Blacksburg, VA 24061, USA

An accurate physics-based transition prediction method integrated with computational fluid dynamics (CFD) solvers is pursued for hypersonic boundary layer flows over slender hypersonic vehicles at flight conditions. The geometry and flow conditions are selected to match relevant trajectory locations from the ascent phase of the HIFiRE-1 flight experiment, namely, a 7-degree half-angle cone with 2.5 mm nose radius, freestream Mach numbers in the range of $3.8 - 5.5$ and freestream unit Reynolds numbers in the range of $3.3 \times 10^6 - 21.4 \times 10^6$ m^{-1}. Earlier research had shown that the onset of transition during the HIFiRE-1 flight experiment correlated with an amplification factor of $N \approx 13.5$ for the planar Mack modes. However, to incorporate the N-factor correlations into a CFD code, we investigate surrogate models for disturbance amplification that avoid the direct computation of stability characteristics. A commonly used approach for low-speed flows is based on an a priori database of stability characteristics for locally similar profiles. However, the results presented in this paper demonstrate that the application of this approach to hypersonic boundary layers over blunt spherical nose-tip cones leads to large, unacceptable errors in the predictions of amplification factors, mainly due to its failure in accounting for the effects of the entropy layer on the boundary-layer profiles along the length of the model. We propose and demonstrate an alternate approach that employs the stability computations for a canonical set of blunt cone configurations to train a physics-informed convolutional neural network model that is shown to provide substantially improved transition predictions for hypersonic flow configurations with entropy-layer effects. Furthermore, the excellent performance of the neural network model is also confirmed for cone configurations with nose radius and half-angle values that do not correspond to those used to build the database. Finally, the convolutional neural network model is shown to outperform the linear stability calculations for underresolved basic states.

Nomenclature

f	=	disturbance frequency [Hz]
h_t	=	total enthalpy [J]
h_ξ	=	streamwise metric factor
h_ζ	=	azimuthal metric factor [m]
L	=	reference length [m]
m	=	azimuthal wavenumber

*Research Engineer, Computational AeroSciences Branch, NASA LaRC. AIAA Senior Member
†Research Engineer, Computational AeroSciences Branch, NASA LaRC. AIAA Senior Member
‡Research Scientist, Computational AeroSciences Branch. AIAA Fellow
§Research Scientist, Computational AeroSciences Branch.
¶Research Scientist, Computational AeroSciences Branch. AIAA Associate Fellow
‖Graduate Student, Aerospace and Ocean Engineering.
**Assistant Professor, Aerospace and Ocean Engineering.

M	=	Mach number
N	=	logarithmic amplification factor
$\bar{\mathbf{q}}$	=	vector of base flow variables
$\tilde{\mathbf{q}}$	=	vector of perturbation variables
$\hat{\mathbf{q}}$	=	vector of amplitude variables
Re_∞	=	freestream unit Reynolds number [m^{-1}]
r_b	=	local radius of axisymmetric body at the axial station of interest [m]
r_n	=	nose radius [m]
t	=	time [s]
T	=	temperature [K]
T_w	=	wall temperature [K]
$T_{w,ad}$	=	adiabatic wall temperature [K]
(u, v, w)	=	streamwise, wall-normal, and spanwise velocity components [m s^{-1}]
(x, y, z)	=	Cartesian coordinates [m]
α	=	streamwise wavenumber [m^{-1}]
β_H	=	Hartree parameter
δ_h	=	boundary layer thickness [m]
κ	=	streamwise curvature [m^{-1}]
ω	=	disturbance angular frequency [rad s^{-1}]
ρ	=	density [kg m^{-3}]
σ	=	growth rate [m^{-1}]
(ξ, η, ζ)	=	streamwise, wall-normal, and azimuthal coordinates [m, m, rad]
θ	=	cone half-angle [rad]
Subscript		
∞	=	freestream value
tr	=	transition location
e	=	boundary-layer edge

I. Introduction

Laminar-turbulent transition of boundary-layer flows can have a strong impact on the performance of hypersonic vehicles because of its influence on the surface skin friction and aerodynamic heating. Therefore, the prediction and control of transition onset and the associated variation of aerothermodynamic parameters in high-speed flows are key issues for optimizing the performance of the next-generation aerospace vehicles. Under low levels of background disturbances, boundary-layer transition is initiated by the exponential amplification of linearly unstable eigenmodes, i.e., modal instabilities of the laminar boundary layer. In two-dimensional boundary layers over sufficiently smooth aerodynamic surfaces, different types of instability mechanisms dominate the exponential growth phase depending on the flight speed. In the incompressible regime, the most amplified disturbances correspond to planar, i.e., two-dimensional, Tollmien-Schlichting (TS) waves, whereas oblique first-mode instabilities are dominant in supersonic boundary layers. The hypersonic regime is again dominated by the growth of planar waves of the second mode, i.e., Mack-mode type [1].

Although many practical aerospace vehicles have blunt, hemispherical and ogival nose tips, the mechanisms that lead to boundary-layer instability and transition on such geometries are often not well understood. A detailed review of boundary-layer transition over sharp and blunt cones in a hypersonic freestream is given by Schneider [2]. As described therein, both experimental and numerical studies have shown that the modal growth of Mack-mode instabilities (or, equivalently, the so-called second-mode waves) is responsible for laminar-turbulent transition on sharp, axisymmetric cones at zero degrees angle of attack. Studies have also shown that increased nose-tip bluntness, i.e., radius of hemispherical or ogival nose tips, lead to the formation of an entropy layer that can extend well beyond the vicinity of the nose-tip region [3]. This entropy layer has been shown to have a stabilizing effect on the amplification of Mack-mode instabilities, which is consistent with the observation that the onset of transition is displaced downstream as the nose bluntness is increased. However, while the boundary-layer flow continues to become more stable with increasing nose bluntness, experiments indicate that the downstream movement in transition actually slows down and eventually reverses as the nose bluntness exceeds a certain critical range of values [3]. The observed reversal in transition onset at large values of nose bluntness is contrary to the predictions from linear stability theory, and therefore, must be explained using a different paradigm. Recently, several efforts have been devoted to studying frustum transition in blunt cones

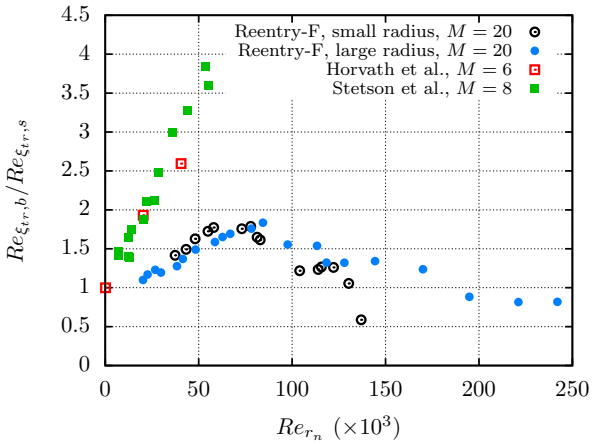

Fig. 1 Ratio of transition Reynolds numbers for blunt cones and the corresponding sharp cone, $Re_{\xi_{tr},b}/Re_{\xi_{tr},s}$, as a function of the nose Reynolds number Re_{r_n}. Data are from the Reentry-F flight experiment at $M = 20$ [9, 10], and ground experiments from Horvath et al. [11] at $M = 6$ and from Stetson et al. [12] at $M = 8$. The $Re_{\xi_{tr},s}$ value is calculated by linear extrapolation.

with the absence of sufficient Mack-mode instability [4–8]. Figure 1 shows the ratio of transition Reynolds numbers for blunt cones and the corresponding sharp cone, $Re_{\xi_{tr},b}/Re_{\xi_{tr},s}$, as a function of the nose Reynolds number Re_{r_n} for the Reentry-F flight experiment at $M = 20$ with a 5-degree half-angle cone [9, 10], and ground experiments reported by Horvath et al. [11] with a 5-degree half-angle cone in the NASA Langley 20-Inch Mach 6 tunnel and by Stetson et al. [12] with a 7-degree half-angle cone in the AEDC Tunnel B at Mach 8 with a 50-Inch diameter test section. The trend is remarkably different between the ground and flight tests, which indicate that the value of $Re_{\xi_{tr},b}/Re_{\xi_{tr},s}$ is affected not only by Re_{r_n}, but also by the freestream conditions and background disturbances. Therefore, an accurate prediction of the transition location will have to account for the bluntness effects on the amplification of Mack-mode instabilities.

Despite neglecting the nonlinear physical processes involved in boundary-layer transition, the linear stability approaches have yielded reasonable estimates for transition onset in a broad class of hypersonic flows (see Refs. [10, 13–15]. Figure 2 shows the evolution of the heat-transfer coefficient for the HIFiRE-1 flight vehicle at $t = 21.5$ s of the ascent phase. The transition location is prescribed using the PSE prediction of Li et al. [14]. However, the procedure to run the stability calculation is decoupled from the computational fluid dynamic (CFD) solver, making the process impractical for design applications.

Direct computations of boundary layer stability place rather stringent demands on the accuracy of mean flow calculations, much more so in comparison with that required for the prediction of aerodynamic metrics such as the skin-friction drag or thermal load. In addition, the solution to the eigenvalue problem associated with the discretized version of the linear stability equations incurs a significant computational cost. Furthermore, due to the complex nature of the eigenvalue spectra and their sensitivity to both input parameters and the numerical discretization, stability computations are difficult to automate, and also require a sufficient expertise by user into the details of the hydrodynamic stability theory. Consequently, the task of transition prediction based on the N-factor methods has been a specialist's domain, also amounting to a single post-processing step that follows the computation of the laminar boundary layer over the flow configuration of interest.

A common approach to circumvent the difficulty with direct computations of the unstable eigenmodes has been to use a database look-up procedure based on a precomputed set of linear stability characteristics of locally similar profiles within the relevant domain of independent parameters [16]. The local boundary-layer characteristics, such as the boundary-layer thickness, pressure gradient, edge Mach number, or wall-to-adiabatic temperature, are evaluated during the CFD run to obtain an interpolated value of the disturbance growth rate from the database. Perraud and Durant [17] investigated this method for Mach 0 to 4.5 conditions with T-S and first mode instabilities, while Pinna et al. [18] focused on a sharp cone at Mach 6. However, this method is not applicable to nonsharp cones, because the effect of the entropy layer is not captured by the self-similar profiles as confirmed later in the present paper. A neural network (NN) based data driven model to predict the disturbance growth characeristics in low-speed flows was first presented by Fuller et al. [19], who applied the model to free-shear flows. However, a significant advance related to transition prediction in swept-airfoil boundary layers was made by Crouch et al. [20], who found that the expressivity of the NN model could

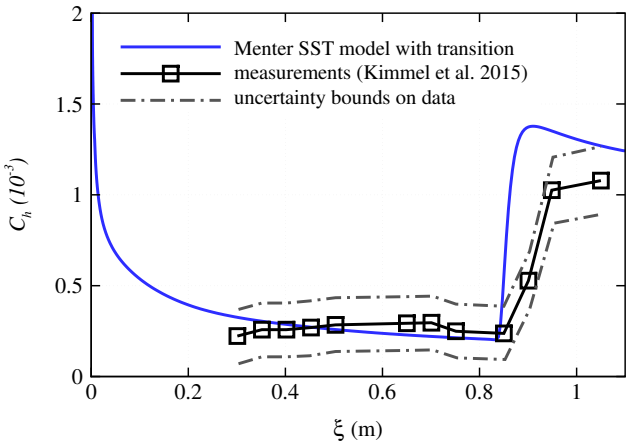

Fig. 2 Streamwise evolution of the heat-transfer coefficient for HIFiRE-1 at t = 21.5 s.

be improved by augmenting the set of scalar variables used in conventional database methods via the slopes of the appropriately normalized velocity profiles at six equidistant points across the boundary layer. The details of the neural network architecture used in that paper are somewhat limited; however, a free-forward network based on fully connected hidden layers was used to approximate the maximum growth rate among all unstable modes at any given station. This maximum growth rate was integrated along the airfoil surface to evaluate the N-factors. The selection of input features in Ref. [20] was somewhat arbitrary and is unlikely to lend itself to other instability mechanisms. A recent extension of the neural network (or, equivalently, deep learning) approach to hypersonic boundary layers over a nominally sharp cone has been presented by Danvin et al. [21, 22]. Even though the neural network performed well in terms of predicting the stability characteristics of the targeted flow configurations, it may be noted that the conventional database look-up procedures have also been highly successful in those cases. In the present work, we present an alternate approach based on a convolutional neural network, also known as a CNN or a ConvNet. As described by Zafar et al. [23], the CNN can automatically learn a reduced order representation of the boundary layer profiles in terms of a specified number of most significant features that can optimally predict the targeted linear stability characteristics across the training space. As such, the proposed architecture can be easily adapted to predict the amplification characteristics of a broad range of very different instability mechanisms.

Given the difficulty in both incorporating and applying stability correlations in CFD solvers, transition models based on the augmentation of Reynolds-averaged Navier-Stokes (RANS) equations are often used for engineering analysis, especially for subsonic flows. The RANS-based transition models do not include the detailed physics related to the amplification of the instability waves that drive the actual boundary-layer transition process. For reasons of computational cost, these models often require that only local information be used to model transition, instead of using detailed boundary layer profiles for stability analysis or even integral boundary layer parameters that may be used in metamodels for the stability characteristics. The RANS-based transition models often rely on solving additional transport equations and using correlations that determine the onset of transition, allowing the codes to switch between operating in the laminar and turbulent modes. An intermittency factor, γ, is usually introduced in the RANS equations to allow for the transitional region. The evolution of γ in the transition region is assumed to be universal in an attached boundary layer within a large range of freestream Reynolds and Mach numbers [24]. The survey of RANS-based models in Fu and Wang [25] divides the RANS-based transition models into three categories: low-Reynolds number turbulence models used as transition models, correlation-based transition models, and models formulated in terms of transport equations involving local variables. Examples of the last class of models include the $k-\omega-\gamma$ model [26, 27], the $\gamma - Re_{\theta t}$ model [28], or the laminar kinetic-energy transition model [29, 30], which all have shown good agreement with the measured data for selected high-speed configurations. However, by virtue of lacking an adequate representation of the complex transition process, such models are also less amenable to an extrapolation to new configurations and must be validated on a case by case basis in general.

The current paper represents a first step toward developing a physics-based transition prediction capability for high-speed flows that is integrated into CFD flow solvers. To that end, the HIFiRE-1 flight database is used to assess the two different surrogate models for linear stability computations. §II provides a summary of the linear stability theory and the convolutional neural network procedure. Results presented in section §III compare predictions using

simple approaches based on Mangler's transformation, or even on similar profiles based on local edge values and a machine-learning approach incorporating a CNN architecture. Finally, summary and concluding remarks are presented in §IV.

II. Theory

This section introduces the methodologies used in this paper.

A. Linear Stability Theory

In what follows, freestream values are used as the reference values for nondimensionalization. The computational coordinates, (ξ, η, ζ), correspond to an orthogonal, body-fitted coordinate system, where ξ denotes the streamwise coordinate measured along the cone surface, η is the surface-normal coordinate, and ζ is measured along the azimuthal direction. The relevant metric factors are defined as

$$h_\xi = 1 + \kappa\eta, \tag{1}$$

$$h_\zeta = r_b + \eta\cos(\theta), \tag{2}$$

where κ denotes the streamwise curvature, r_b is the local radius, and θ is the local half-angle along the axisymmetric surface, i.e., $\sin(\theta) = \mathrm{d}r_b/\mathrm{d}\xi$. For the present straight circular cone (with exception of the nose region that is not included in this analysis), $\kappa \equiv 0$.

The instability characteristics of the axisymmetric boundary layer over the cone is calculated with quasiparallel linear stability theory (LST), which assumes the boundary-layer profiles to be locally parallel by dropping the streamwise derivative terms and setting the wall-normal velocity equal to zero. In the LST context, the perturbations have the form

$$\tilde{\mathbf{q}}(\xi, \eta, \zeta, t) = \hat{\mathbf{q}}(\eta)\exp\left[\mathrm{i}\left(\alpha\xi + m\zeta - \omega t\right)\right]. \tag{3}$$

The suitably nondimensionalized, orthogonal, curvilinear coordinate system (ξ, η, ζ) denotes streamwise, wall-normal, and azimuthal coordinates, respectively, and (u, v, w) represents the corresponding velocity components. Density and temperature are denoted by ρ and T. The Cartesian coordinates are represented by (x, y, z). The vector of perturbation fluid variables is $\tilde{\mathbf{q}}(\xi, \eta, \zeta, t) = (\tilde{\rho}, \tilde{u}, \tilde{v}, \tilde{w}, \tilde{T})^T$, the vector of amplitude functions is $\hat{\mathbf{q}}(\eta) = (\hat{\rho}, \hat{u}, \hat{v}, \hat{w}, \hat{T})^T$, and the vector of basic state fluid variables is $\bar{\mathbf{q}}(\eta) = (\bar{\rho}, \bar{u}, \bar{v}, \bar{w}, \bar{T})^T$. The streamwise and azimuthal wavenumbers are α and m, respectively, and ω is the angular frequency of the perturbation. The azimuthal wavelength is defined as $\lambda = 2\pi/m$. Substituting Eq. (3) into the linearized NS equations, an ordinary-differential-equation (ODE) based generalized eigenvalue problem (GEVP) can be written in the following form by using the companion matrix method [31] to reduce the quadratic terms in α from the viscous terms,

$$\mathbf{A}\hat{\mathbf{q}}^+ = \alpha\mathbf{B}\hat{\mathbf{q}}^+, \tag{4}$$

where $\hat{\mathbf{q}}^+(\eta) = (\hat{\rho}, \hat{u}, \hat{v}, \hat{w}, \hat{T}, \alpha\hat{u}, \alpha\hat{v}, \alpha\hat{w}, \alpha\hat{T})^T$. The entries of operators $\mathbf{A}$ and $\mathbf{B}$ are found in Refs. [13, 32]. The GEVP is solved by the inverse Rayleigh iteration method [33]. The imaginary part of the eigenvalue α represents the damping rate of the instability wave, and therefore, the growth rate is calculated as

$$\sigma = -\Im(\alpha). \tag{5}$$

The onset of laminar-turbulent transition is estimated using the logarithmic amplification ratio, the so-called N-factor, relative to the lower bound location ξ_{lb} where the disturbance first becomes unstable,

$$N = \int_{\xi_{lb}}^{\xi} \sigma(\xi')\,\mathrm{d}\xi'. \tag{6}$$

Accordingly, we assume that transition onset is likely to occur when the peak N-factor reaches a specified value.

B. Physics-Informed Convolutional Neural Network

Neural networks are a sequence of composite functions, which represent mappings from input $\mathbf{p}$ to output $\mathbf{y}$, and are parametrized by weights $\mathbf{W}$ and biases $\mathbf{b}$ that can be learned using available training data. Such sequences of composite

functions is arranged in form of layers, where an NN with one intermediate (hidden) layer between input and output layers may be represented by the following composite functional mapping:

$$\mathbf{y} = \mathbf{W}^{(2)}\mathbf{h} + \mathbf{b}^{(2)}, \tag{7}$$

$$\mathbf{h} = \lambda(\mathbf{W}^{(1)}\mathbf{p} + \mathbf{b}^{(1)}), \tag{8}$$

where λ is an activation function, $\mathbf{W}^{(i)}$ and $\mathbf{b}^{(i)}$ represent weights' matrix and biases vector for $\mathbf{i}^{th}$-layer. Activation functions introduce the much-needed complexity/nonlinearity in the composite functions of NNs, which enables them to represent complex mappings. Activation functions can be represented by sigmoid function $\lambda(x) = 1/(1 + e^{-x})$ or rectifier linear unit (ReLU), $\lambda(x) = \max(0, x)$. Neural network with multiple hidden layers is generally termed as deep NN.

Fully connected NNs have each neuron connected to every neuron in the previous layer, which is a general-purpose connection pattern which makes no assumptions about the input features in the data. A fully connected NN is also more expensive in terms of memory and computation. In comparison, CNNs make use of a number of attributes to learn efficiently with lower number of model parameters. In the CNN model, each neuron is firstly locally connected to several neurons in the previous layer to develop a correlation with neighboring neurons. Secondly, the convolutional kernel has a translational invariance in terms of model parameters. Such attributes allow CNN to achieve comparable performance much more efficiently [34].

CNN is composed of number of convolutional layers and pooling layers, followed by fully connected layers. For the details of the CNN (or ConvNet) architecture used in this paper, the reader is referred to Zafar et al. [23], who showed how this architecture provides a flexible approach to predict linear stability characteristics by learning the relevant features of the mean boundary-layer profiles. The present work is based on a conceptually similar extension of that approach to the Mack mode instability in high Mach number flows. Specifically, we introduce the locally nondimensionalized disturbance frequency $\omega_e = \omega\delta_h/u_e$ and the Reynolds number $Re_{\delta_h} = \rho_e u_e \delta_h/\mu_e$, where the subscript e denotes the value at the boundary-layer edge, into fully connected layers. The boundary-layer edge is defined as the wall-normal position where $h_t/h_{t,\infty} = 0.995$, with h_t denoting the total enthalpy, i.e., $h_t = h + 0.5(\bar{u}^2 + \bar{v}^2 + \bar{w}^2)$, where h is the static enthalpy. The azimuthal wavenumber was not introduced because it is set to zero for the planar Mack waves of interest to the present work. The convolutional and pooling layers mapped the boundary-layer profiles to physical quantity space. The physical quantities are then nonlinearly mapped to instability growth rate as final output. This extended network architecture is referred to as physics-informed CNN. The dependence of physical parameters ω_e and Re_{δ_h} was introduced into the network architecture in an explicit yet flexible manner. That is, the dependency of instability growth rate on ω_e and Re_{δ_h} along with boundary-layer profiles is known and their exact relation can be inferred by training. While ω_e and Re_{δ_h} appears to be the preferred choice, other choices of input parameters have also been tested in the current study with different combinations of boundary-layer profiles.

The convolutional NN architecture is chosen to minimize the mean squared error in growth rate predictions for the training database, which corresponds to a randomly sampled subset of the overall data. Convolutional kernels of size 3 x 1 are used for feature extraction from the boundary layer profiles sampled at 60 equidistant points from the surface. The CNN distills the information from these boundary-layer profiles to identify a smaller number of parameters that are used, along with four scalar input features, as the input to the fully connected layers. A total of seven layers are used in the fully connected portion of the network and ReLU are used as activation functions throughout the network. The number of fully connected layers is selected empirically, to ensure a sufficiently expressive neural network that is able to learn all of the required information without causing an overfitting of the data. The above CNN architecture has been implemented by using the machine learning framework PyTorch.

III. Results

The basic state approximations to the axisymmetric boundary layer over a circular cone at zero degrees angle of attack in a hypersonic free stream are presented first. Quasiparallel linear stability theory (LST) is used to calculate the instability characteristics of the selected basic state approximations, namely, the laminar Navier-Stokes (NS) solution, a sharp-cone self-similar solution based on Taylor-Maccoll (TM) post-shock conditions and the Mangler transformation, and self-similar solutions that locally match the boundary-layer-edge (LE) characteristics and boundary-layer thickness of the Navier-Stokes solution. Then, the performance of the physics-informed convolutional NN based on a database composed by LST results for laminar NS solutions is evaluated.

A. Basic State Approximations

The flow configuration of interest corresponds to the HIFiRE-1 geometry, specifically, a 7° half-angle, circular cone at zero-degrees angle of attack in a hypersonic free stream. The length of the cone is $L_c = 1.0$ m, and the nose radius is $r_n = 2.5$ mm. The basic state corresponding to the laminar boundary-layer flow over the cone surface is computed by using a second-order accurate algorithm as implemented in the finite-volume compressible Navier-Stokes flow solver VULCAN-CFD* [35]. The VULCAN-CFD solution is based on the full Navier-Stokes equations and uses the solver's built-in capability to iteratively adapt the computational grid to the shock. Sutherland's law is assumed for bulk viscosity.

The freestream conditions are selected to replicate those of the HIFiRE-1 flight experiment during the ascent phase [36]. The specific conditions for the selected times and the corresponding measured transition locations are shown in Table 1. The imposed surface temperature distribution was obtained by combining the results of thermal analysis based on axisymmetric, finite-element calculations using the AFRL TOPAZ code [37] and the experimental data based on thermocouple measurements [36]. Li et al. [14] present a thorough stability analysis of the flight experiment. Figure 3(a) shows the prescribed distribution of surface temperature along the length of the cone for $t = 21.5$ s.

Table 1 Freestream conditions at selected times during ascent phase of HIFiRE-1 vehicle and measured transition locations [14].

Time (s)	$\bar{p}_\infty$ (Pa)	$\bar{T}_\infty$ (K)	M_∞	Re_∞ (10^6 m^{-1})	Altitude (km)	ξ_{tr} (m)
17.5	16,416.3	213.4	3.82	21.37	13.66	–
18.0	15,011.2	209.9	4.10	21.44	14.22	–
19.0	12,317.9	205.3	4.66	20.58	15.42	0.672
20.0	9,851.9	201.0	5.07	18.46	16.75	0.708
21.5	6,878.1	201.4	5.30	13.42	18.86	0.847
22.0	6,102.5	203.7	5.31	11.74	19.58	0.929
23.0	4,811.9	209.2	5.31	8.93	21.03	–
25.0	3,014.7	219.6	5.36	5.29	24.00	–
27.0	1,886.1	225.0	5.41	3.29	27.07	–

The computational grid has 865 points in the streamwise direction and 513 points in the wall normal direction. A minimum of 120 points is clustered next to the cone surface to resolve the thickness of the boundary layer. This grid resolution is based on the work of Li et al. [14], who computed the laminar flow over the HIFiRE-1 geometry at selected instances of times during the flight experiment by using the VULCAN-CFD flow solver. They also performed a grid-convergence test by doubling the number of points in each direction, and furthermore, verified the results by comparing the solution with that computed with a different Navier-Stokes solver in the form of the CFL3D code [38].

The edge Mach number M_e and boundary-layer thickness δ_h are plotted in Figs. 3(b) and 3(c), respectively, for the flight time $t = 21.5$ s. Besides the NS solution, the boundary-layer solution corresponding to a sharp cone with the same freestream conditions, which are related to boundary-layer-edge values through the Taylor-Maccoll (TM) equations, is also used with a constant wall temperature of $T_w = 393.44$ K that corresponds to a wall-to-adiabatic temperature of $T_w/T_{w,ad} = 0.34$. Figure 3(b) shows how the edge Mach number of the NS solution nearly coincides with that of the TM solution for $\xi > 0.2$ m, however, Fig. 3(c) shows that the boundary-layer thickness of the TM solution does not match the NS solution within the length of the cone. Therefore, two boundary-layer solutions composed by self-similar profiles that match the local edge (LE) values and boundary-layer thickness of the NS solution have been calculated, one locally assuming a zero-pressure gradient through selecting the Hartree parameter equal to zero ($\beta_H = 0$) and one including the local pressure gradient effects with $\beta_H \neq 0$, as made by Perraud and Durant [17]. The streamwise velocity and temperature profiles with the four approaches are compared in Fig. 4 at $\xi = 0.2$, 0.4, 0.6, and 0.8 m. The profiles based on LE values agree better than the TM solution, but the profile comparisons show clear differences in the vicinity of the boundary-layer edge even for $\xi = 0.8$ m. Therefore, the effect of the entropy layer generated by the blunt nose tip extends over the length of the cone, although, as shown in Fig. 3(b), the edge Mach number coincides with the sharp cone solution for $\xi > 0.2$ m.

*visit `http://vulcan-cfd.larc.nasa.gov` for further information about the VULCAN-CFD solver

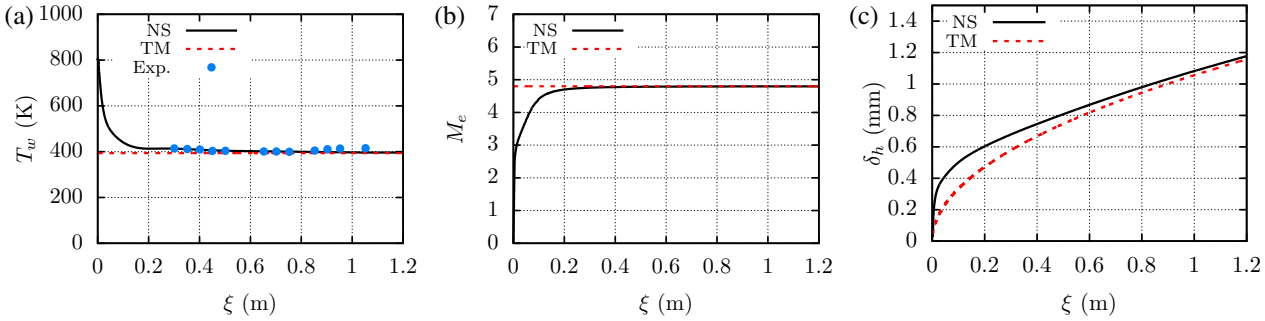

Fig. 3 Streamwise evolution of (a) wall temperature, (b) edge Mach number, and (c) boundary layer thickness for the Navier-Stokes (NS) and sharp-cone self-similar based on Taylor-Maccoll (TM) solutions. The wall temperature values measured in the flight experiments are included.

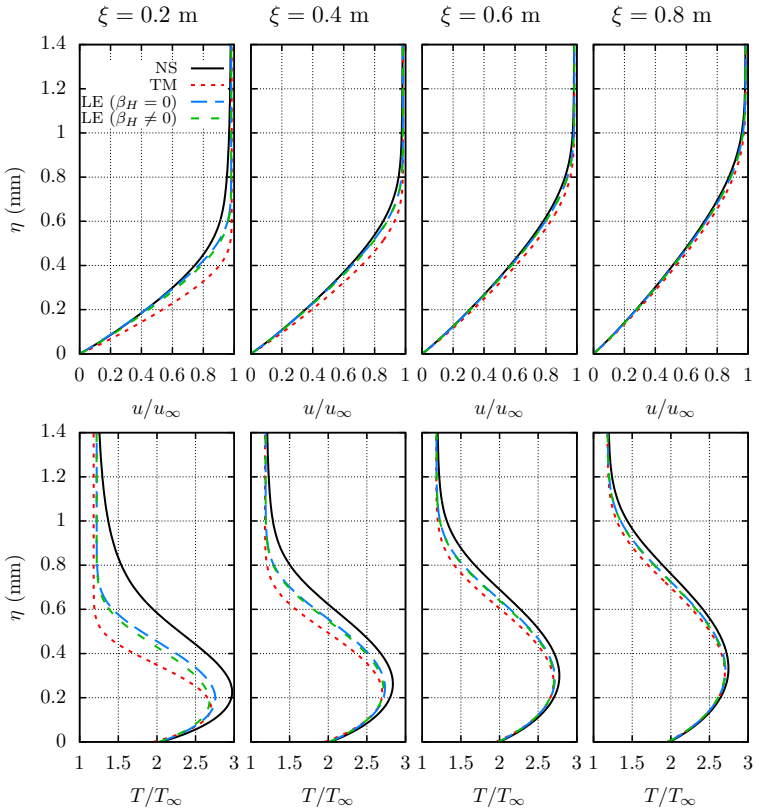

Fig. 4 Comparison of streamwise velocity and temperature profiles for the Navier-Stokes (NS) and self-similar solutions based on local edge (LE) values with $\beta_H = 0$ and $\beta_H \neq 0$.

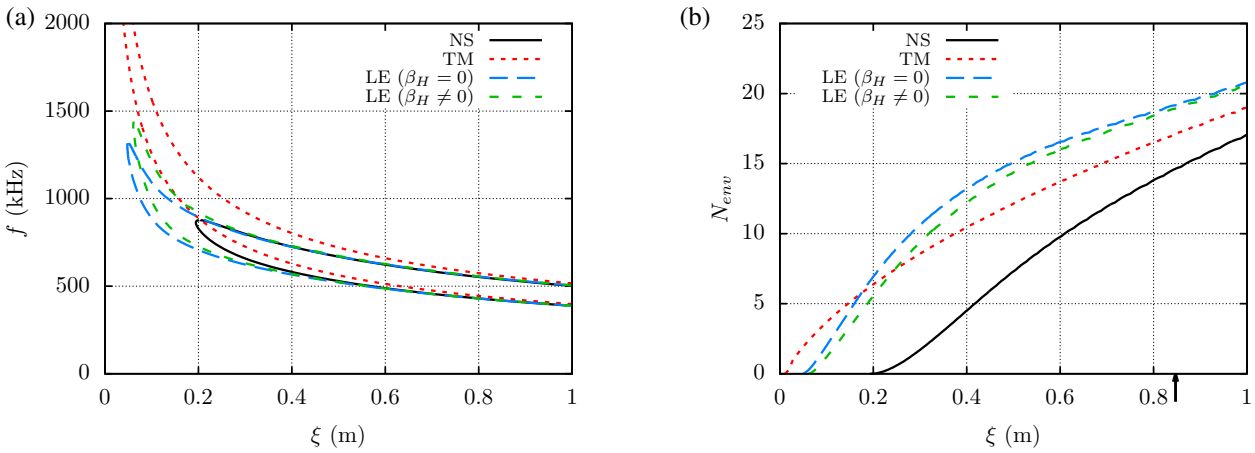

Fig. 5 (a) Neutral curves and (b) N-factor envelopes of planar Mack-mode disturbances for the HIFiRE-1 vehicle at flow conditions corresponding to a flight ascent time of $t = 21.5$ s.

B. Instability Characteristics

Experimental measurements and theoretical predictions based on the parabolized stability equations (PSE) have confirmed that laminar-turbulent transition in this flow is driven by the modal growth of planar Mack-mode instabilities [14]. For the conditions of the experiment at $t = 21.5$ s, transition onset in the cone was measured to occur near $\xi_{tr} = 0.847$ m. The peak N-factor at the measured transition location was calculated with the parabolized stability equations by Li et al. [14] and resulted in an $N_{tr} = 14.51$. The peak N-factor is first reached by a planar Mack-mode disturbance with a frequency of $f = 530$ kHz. Here, the quasiparallel LST is used to calculated the instability characteristics of the flow field, because the nonparallel effects are negligible for this configuration. Quasiparallel LST gives an N-factor of $N = 14.63$ at $\xi_{tr} = 0.847$ m. Figure 5(a) shows the neutral stability curve for the selected basic flow approaches. Neither planar nor oblique first-mode instabilities were found to be unstable in the present boundary-layer flow because of the low surface temperature relative to the adiabatic temperature. The neutral stability curves show that the onset of Mack-mode instabilities for the basic state solutions based on self-similar profiles is significantly upstream in comparison with the profiles based on the NS solution. The discrepancy between the TM and NS solutions in regard to the range of unstable frequencies is corrected by the LE solutions. However, Fig. 5(b) shows that the N-factor values for the LE solutions are higher than those corresponding to TM and NS basic state solutions. The addition of the favorable pressure gradient through the Hartree parameter reduces the N-factor values, but only slightly, and the disagreement with the NS solution remains unacceptable. Using the same transition N-factor of $N_{tr} = 14.63$, the predicted transition location for the LE solution with $\beta_H \neq 0$ has a relative error of 39.3%. On the other hand, the sharp-cone solution based on TM post-shock conditions lead to a relative error of 21.7%. It is worth noting that the blunt-to-sharp transition Reynolds number ratio for the present configuration with $Re_{R_N} = 33,550$ is equal to $Re_{\xi_{tr},b}/Re_{\xi_{tr},s} = \xi_{tr,b}/\xi_{tr,s} = 1.31$, which is consistent with the Reentry-F flight data from Fig. 1. The different slopes for the ground and flight data in Fig. 1 could be related to the different associated transition N-factor. Figure 5(b) shows that for $N_{tr} = 5$, which is a typical value for ground experiments in conventional hypersonic tunnels, the blunt-to-sharp transition Reynolds number ratio would be $Re_{\xi_{tr},b}/Re_{\xi_{tr},s} = 2.88$; this ratio is also consistent with the ground experiment data from Fig. 1.

The large discrepancies in N-factor envelopes between the basic state solutions observed in Fig. 5(b) is further examined in Fig. 6 by comparing the growth-rate spectra at selected streamwise locations. The growth rates for the TM and the LE basic states are consistently larger than those for the NS basic state. The N-factor envelope for the TM solution shows a closer agreement with that of the NS solution, but the frequency range of the Mack-mode instabilities is remarkably different from the NS case.

C. Performance of the Physics-Informed Convolutional Neural Network

Herein, the results assessing the predictive performance of the machine learning model are presented. The database is composed of the LST results for 693 basic states calculated with the VULCAN-CFD solver for the HIFiRE-1 circular cone at freestream conditions corresponding to $M_\infty = 4.0 : 0.25 : 6.0$, $\bar{T}_\infty = 200$ K, and $\bar{p}_\infty = 6,000 : 2,000 : 18,000$

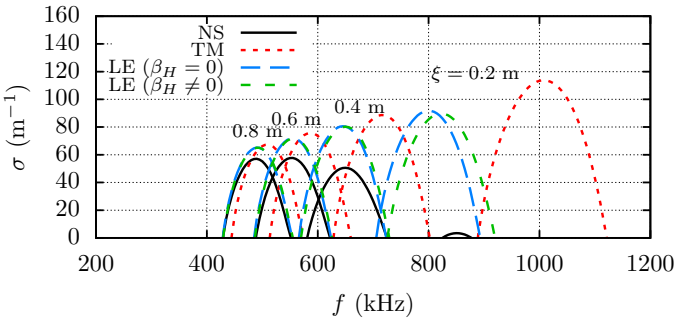

Fig. 6 Growth rates of planar Mack-mode disturbances for the HIFiRE-1 vehicle at flow conditions corresponding to a flight ascent time of $t = 21.5$ s

Pa, and a constant wall temperature of $\bar{T}_{wall} = 300 : 50 : 800$ K. The database includes the parameters that define the boundary layer profiles, namely, ξ/r_n, δ_h (m), $\bar{u}_e$ (m/s), $\bar{T}_e$ (K), $\bar{\rho}_e$ (kg/m^3), Re_{δ_h}, M_e, and the values of boundary layer profiles at 61 equispaced points from the wall to $\eta = 3\delta_h$. For every streamwise station, the disturbance frequency $\omega * \delta_h/\bar{u}_e$ and the corresponding growth rate $\sigma * \delta_h$ calculated with quasiparallel LST with disturbance frequency increments of $\Delta f = 5$ kHz. In total, the database contains nearly 4.41×10^6 entries.

The performance of the convolutional NN is first evaluated for the HIFiRE-1 vehicle at the selected times during ascent phase shown in Table 1. Figure 7 shows the comparison of the N-factor curves with disturbance frequencies of $\Delta f = 10$ kHz between the LST results and the NN predictions. The agreement is excellent for all cases, and small discrepancies are distinguishable only in Figs. 7(a) and 7(i), for times $t = 17.5$ s and $t = 27.0$ s, respectively. However, the flow conditions of these two cases lie outside the database conditions, because the freestream Mach number at $t = 17.5$ s is $M_\infty = 3.82$, while the minimum value in the database is $M_\infty = 4.0$, and the freestream pressure at $t = 27.0$ s is $P_\infty = 1,886.1$ Pa, while the minimum value in the database is $P_\infty = 6,000$ Pa. Therefore, we expect that the small differences observed in Figs. 7(a) and 7(i) can be easily reduced by extending the database to include a broader set of freestream conditions.

The applicability of the NN predictive capability of planar Mack mode amplification to different configurations is explored next. Figure 8 shows the high level of agreement for four circular cones with a half-angle of 7°, as the HIFiRE-1 vehicle, but with nose radii equal to $r_n = 0.5\,r_{n,0}$, $1.5\,r_{n,0}$, $2.0\,r_{n,0}$, and $4.0\,r_{n,0}$, where $r_{n,0} = 2.5$ mm corresponds to the nose radius of the HIFiRE-1 vehicle. The freestream flow conditions corresponds to the HIFiRE-1 flight time of $t = 20.0$ s. Therefore, the NN based on a constant nose radius and selected freestream conditions is able to predict the downstream movement of the transition location as the nose radius is increased. Figure 9 shows a similar assessment for a circular cone with a smaller half-angle of 5° and a nose radius of $r_n = 2.5$, as the HIFiRE-1 vehicle for freestream conditions corresponding to $t = 20.0$ s (Fig. 9(a)) and $t = 21.5$ s (Fig. 9(b)). For both conditions, the performance of the NN is excellent.

For the comparisons shown in Figs. 7, 8, and 9, the excellent accuracy of the CNN predictions in relation to ground truth predictions is not limited to the small number of modes that determine the onset of transition on the bases of the N-factor correlation, but it seems to cover most of the parameter space where the Mack mode instability is present.

Finally, the robustness of the convolutional NN is evaluated by using underresolved basic state solutions of the boundary layer over the HIFiRE-1 vehicle at freestream conditions corresponding to the flight ascent time of $t = 20.0$ s. The quality of the basic state solution is deteriorated by switching off the shock adaptation process ("no adapt."), by reducing the discretization order from second to first order ("1^{st}"), and by reducing the number of points in the wall-normal direction by half ("$n_\eta/2$") and by four ("$n_\eta/4$"). Figure 10 shows the comparison of N-factor envelopes calculated with LST using the original solution (NS) and the underresolved solutions, and the prediction of the NN model based on the inputs from the underresolved solutions. A similar comparison for the analogous case with no shock adaptation but second-order discretization is not shown here because no significant differences were observed relative to the ground truth predictions. Surprisingly, the prediction of the physics-informed convolutional NN model outperforms the LST results based on the underresolved basic state solutions, which reflects that the NN model is less sensitive to the accuracy of the basic state definition than the actual stability computations. Table 2 shows the relative error in transition location for the LST results (NS) and the NN model using the four underresolved basic state solutions. As expected, the LST error increases as the accuracy of the basic state solution decreases, yielding an error of nearly 8% for the solution with no shock adaptation, first discretization order and one fourth the number of wall-normal points with respect to the

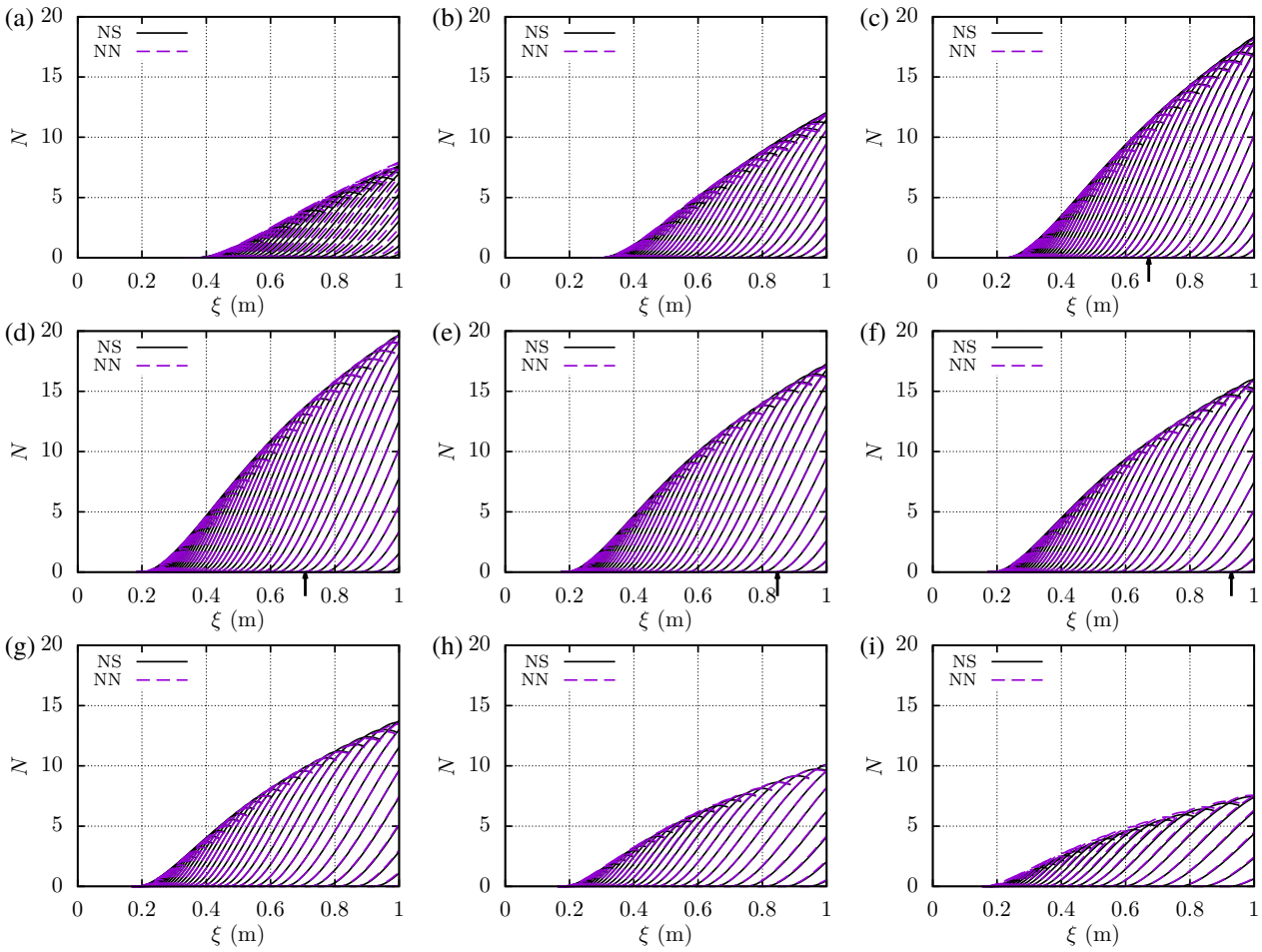

Fig. 7 N**-factor curves for planar Mack-mode disturbances over the HIFiRE-1 vehicle at flow conditions corresponding to flight ascent times: (a)** $t = 17.5$ **s, (b)** $t = 18.0$ **s, (c)** $t = 19.0$ **s (**$\xi_{tr} = 0.672$ **m), (d)** $t = 20.0$ **s (**$\xi_{tr} = 0.708$ **m), (e)** $t = 21.5$ **s (**$\xi_{tr} = 0.847$ **m), (f)** $t = 22.0$ **s (**$\xi_{tr} = 0.929$ **m), (g)** $t = 23.0$ **s, (h)** $t = 25.0$ **s, and (i)** $t = 27.0$ **s. The vertical arrow indicate the transition location.**

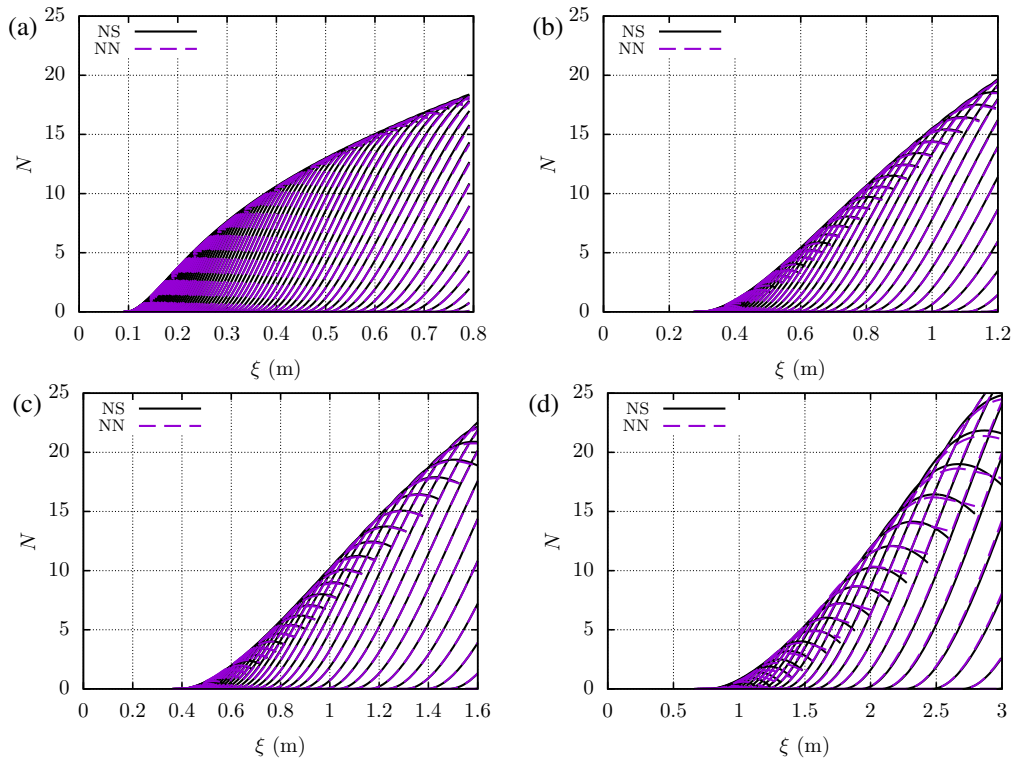

Fig. 8 N**-factor curves for planar Mack-mode disturbances over a** 7° **half-angle cone with a nose radius of (a)** $r_n = 0.5\,r_{n,0}$**, (b)** $r_n = 1.5\,r_{n,0}$**, (c)** $r_n = 2.0\,r_{n,0}$**, and (d)** $r_n = 4.0\,r_{n,0}$**, where** $r_{n,0} = 2.5$ **mm, at flow conditions corresponding to a flight ascent time of** $t = 20.0$ **s.**

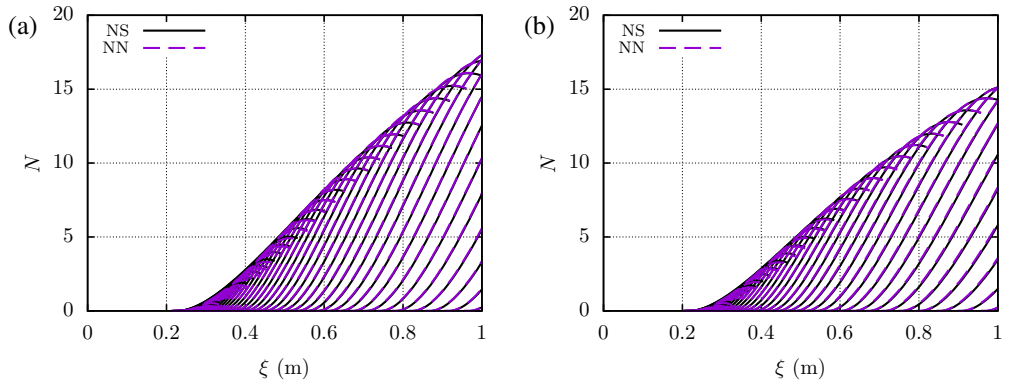

Fig. 9 N**-factor curves for planar Mack-mode disturbances over a** 5° **half-angle cone with a nose radus of** $r_n = 2.5$ **mm and at flow conditions corresponding to a flight ascent time of (a)** $t = 20.0$ **s and (b)** $t = 21.5$ **s.**

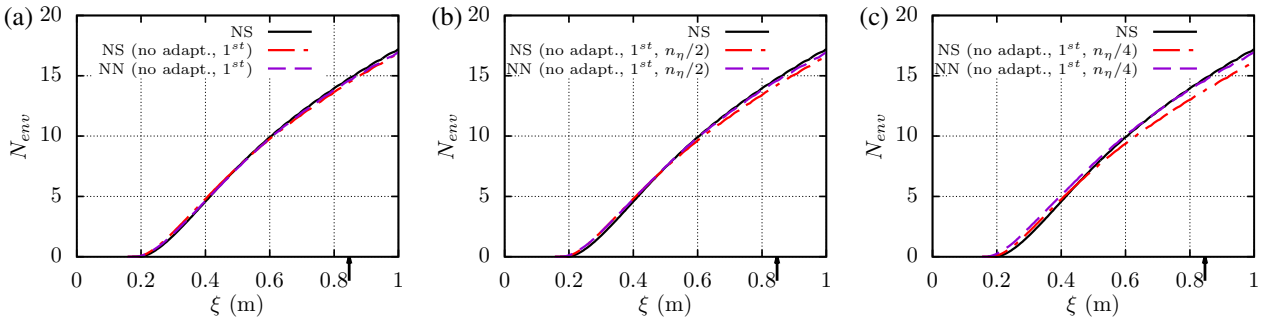

Fig. 10 **N-factor envelopes for planar Mack-mode disturbances over the HIFiRE-1 vehicle at flow conditions corresponding to a flight ascent time of t = 21.5 s and selected numerical methods: "no adapt." refers to no shock adaptation, "1^{st}" refers to first order finite-volume discretization, "$n_\eta/2$" refers to a reduction of the number of points along the wall-normal direction by half, and "$n_\eta/4$" refers to a reduction by four.**

converged solution. However, the relative error of the NN predictions remains below 2% for all of these cases.

Table 2 Performance of physics-informed convolutional NN model with underresolved basic state solutions.

Numerical Method	ϵ_{NS} (%)	ϵ_{NN} (%)
no adapt.	0.24	0.25
no adapt., 1^{st}	2.60	1.48
no adapt., 1^{st}, $n_\eta/2$	4.13	1.43
no adapt., 1^{st}, $n_\eta/4$	7.67	1.14

IV. Summary and Concluding Remarks

Boundary-layer transition modeling approaches based on stability analysis for hypersonic boundary layers at representative flight conditions are investigated. First, the boundary-layer transition predictions based on quasiparallel linear stability theory (LST) for self-similar boundary-layer profiles are compared with LST results for the laminar Navier-Stokes boundary-layer flow over the HIFiRE-1 flight experiment configuration, namely, a 7° half-angle cone with 2.5 mm nose radius at flight ascent time of t = 21.5 s. The simplified boundary-layer flows are calculated for an equivalent sharp cone using Taylor-Maccoll relations, and for locally equivalent edge values and boundary-layer thickness with and without local pressure gradient effects. The comparison of streamwise velocity and temperature profiles show how the entropy layer introduced by the blunt nose-tip extends along the vehicle and leads to modified profiles that are not fully corrected by the local boundary-layer edge properties and thickness. Although the LST results for the profiles that match the local boundary-layer properties also match the unstable frequency range of Mack-mode instabilities, the predicted growth rates are consistently larger than for those calculated with the Navier-Stokes solution, resulting in transition onset predictions that are in error by approximately 40%. Therefore, the use of stability analysis results based on self-similar profiles is not appropriate for realistic blunt geometries.

A machine learning approach based on physics-informed convolutional neural network (CNN) trained on LST calculations for the laminar boundary layer over a 7° half-angle cone with with 2.5 mm nose radius at selected freestream conditions (M_∞ = 4.0 : 0.25 : 6.0, $\bar{T}_\infty$ = 200 K, and $\bar{p}_\infty$ = 6,000 : 2,000 : 18,000 Pa) and an isothermal surface corresponding to $\bar{T}_w$ = 300 : 50 : 8004 K is shown to alleviate the shortcomings of the local similarity model and provide substantially improved transition predictions for hypersonic flow configurations with moderate entropy layer effects. The performance of the NN model is evaluted for a broad range of the HIFiRE-1 flight ascent phase times, as well as for alternate circular cone geometries with a half-angle of 5° and nose radii of 1.25, 3.75, 5.0, and 10.0 mm. For all configurations, the agreement between the NN model predictions and the LST results is excellent. Furthermore, the NN model is shown to outperform the LST calculations when the basic state solution is underresolved by not invoking shock adaptation, reducing the discretization order from second to first, and by reducing the number of wall-normal points.

The present study provides a preliminary proof of concept to establish the feasibility of accurate, robust, yet higly efficient stability predictions via the deep learning approach. We note that stability computations for axisymmetric cones can be performed in a relatively straighforward manner. However, the deep learning approach is found to generalize well to cones with nonuniform surface temperature distributions, a different cone angle in comparison with the 7° half-angle cone used during training, and even to freestream conditions that amount to an extrapolation beyond the parameter space covered by the training space. Thus, with limited extra validation, it is quite possible that the present model or a modification thereto based on transfer learning would also apply to other flow configurations involving the Mack mode instability. Another benefit of this model is that the prediction of the disturbance growth rates requires little expertise on the user's part, making physics-based transition prediction accessible to nonexpert users. On a practical front, the highly efficient transition predictions based on this model can be used for accurate estimations of the temporal variations in the heat load on the vehicle as the latter flies through various candidate trajectories, making it a useful, physics-based tool during trajectory analysis. The follow-on efforts will focus on the integration of the stability-based transition model within a CFD computation for an automated prediction of the transition location.

Acknowledgments

This research was sponsored by the NASA Transformational Tools and Technologies (TTT) Project of the Transformative Aeronautics Concepts Program (TACP) under the Aeronautics Research Mission Directorate (ARMD). A portion of the computational resources supporting this work were provided by the NASA High-End Computing (HEC) Program through the NASA Advanced Supercomputing (NAS) Division at the Ames Research Center.

References

[1] Mack, L., "Boundary Layer Linear Stability Theory," *AGARD–R–709 Special course on stability and transition of laminar flow*, 1984, pp. 3.1–3.81.

[2] Schneider, S., "Hypersonic Laminar-Turbulent Transition on Circular Cones and Scramjet Forebodies," *Progress in Aerospace Sciences*, Vol. 40, 2004, pp. 1–50. doi:10.1016/j.paerosci.2003.11.001.

[3] Stetson, K., "Nosetip Bluntness Effects on Cone Frustum Boundary Layer Transition in Hypersonic Flow," AIAA Paper 83-1763, 1983. doi:10.2514/6.1983-1763.

[4] Marineau, E., Moraru, C., Lewis, D., Norris, J., Lafferty, J., Wagnild, R., and Smith, J., "Mach 10 Boundary-Layer Transition Experiments on Sharp and Blunted Cones," AIAA Paper 2014-3108, 2014. doi:10.2514/6.2014-3108.

[5] Paredes, P., Choudhari, M., Li, F., Jewell, J., Kimmel, R., Marineau, E., and Grossir, G., "Nosetip Bluntness Effects on Transition at Hypersonic Speeds: Experimental and Numerical Analysis," *Journal of Spacecraft Rockets*, Vol. 56, No. 2, 2019. doi:10.2514/1.A34277.

[6] Paredes, P., Choudhari, M., Li, F., Jewell, J., and Kimmel, R., "Nonmodal Growth of Traveling Waves on Blunt Cones at Hypersonic Speeds," *AIAA Journal*, Vol. 57, No. 11, 2019, pp. 4738–4749. doi:10.2514/1.J058290.

[7] Paredes, P., Choudhari, M., and Li, F., "Laminar-Turbulent Transition Upstream of the Entropy-Layer Swallowing Location in Hypersonic Boundary Layers," AIAA Paper 2019-3215, 2019. doi:10.2514/6.2019-3215.

[8] Kennedy, R., Jagde, E., Laurance, S., Jewell, J., and Kimmel, R., "Visualizations of Hypersonic Boundary-Layer Transition on a Variable Bluntness Cone," AIAA Paper 2019-3079, 2019. doi:10.2514/6.2019-3079.

[9] Wright, R., and Zoby, E., "Flight Boundary Layer Transition Measurements on a Slender Cone at Mach20," AIAA Paper 77-719, 1977.

[10] Lau, K., "Hypersonic Boundary-Layer Transition: Application to High-Speed Vehicle Design," *Journal of Spacecraft Rockets*, Vol. 45, No. 2, 2008, pp. 176–183.

[11] Horvath, T., Berry, S., Hollis, B., Chang, C.-L., and Singer, B., "Boundary Layer Transition on Slender Cones in Conventional and Low Disturbance Mach6 Wind Tunnels," AIAA Paper 2002-2743, 2002. doi:10.2514/6.2002-2743.

[12] Stetson, K., Thompson, E., Donaldson, J., and Siler, L., "Laminar Boundary Layer Stabiltiy Experiments on a Cone at Mach 8, PART 2: Blunt Cone," AIAA Paper 84-0006, 1984. doi:10.2514/6.1984-0006.

[13] Malik, M. R., "Numerical Methods for Hypersonic Boundary Layer Stability," *Journal of Computational Physics*, Vol. 86, 1991, pp. 376–413.

[14] Li, F., Choudhari, M., Chang, C., Kimmel, R., Adamczak, D., and Smith, M., "Transition Analysis for the Ascent Phase of HIFiRE-1 Flight Experiment," *Journal of Spacecraft Rockets*, Vol. 52, No. 5, 2015, pp. 1283–1293.

[15] Tufts, M., Gosse, R., and Kimmel, R., "Parabolized Stability Equatino Analysis of Crossflow Instability on HIFiRE-5b Flight Test," *Journal of Spacecraft Rockets*, Vol. 56, No. 6, 2018, pp. 1–10.

[16] van Ingen, J., "The e^N Method for Transition Prediction. Historical Review of Work at TUDelf," AIAA Paper 2008-3830, 2008.

[17] Perraud, J., and Durant, A., "Stability-Based Mach Zero to Four Longitudinal Transition Prediction Criterion," *Journal of Spacecraft Rockets*, Vol. 56, No. 6, 2018, pp. 1–10.

[18] Pinna, F., Zanus, L., Demange, S., and Olazabal-Loume, M., "Reduced Model for Transition Prediction in Hypersonic Flows," AIAA Paper 2018-3697, 2018.

[19] Fuller, R., Saunders, W., and Vandsburger, U., "Neural Network Estimation of Disturbance Growth using a Linear Stability Numerical Model," AIAA Paper 97-3701, 1997.

[20] Crouch, J., Crouch, I., and Ng, L., "Transition Prediction for Three-Dimensional Boundary Layers in Computational Fluid Dynamics Applications," *AIAA Journal*, Vol. 40, No. 8, 2002, pp. 1536–1541.

[21] Danvin, F., Pinna, F., and Olazabal-Loume, M., "Laminar-To-Turbulent Transition Prediction in Hypersonic Flows with Metamodels," AIAA Paper 2018-3701, 2018.

[22] Danvin, F., , Olazabal, M., and Pinna, F., "Laminar to Turbulent Transition Prediction in Hypersonic Flows with Neural Networks Committee," AIAA Paper 2019-2837, 2019.

[23] Zafar, M., Xiao, H., Paredes, P., Venkatachari, V., Choudhari, M., Li, F., and Chang, C.-L., "Predicting Laminar-Turbulent Transition with Physics-Informed Convolutional Neural Network," *Theoretical and Computational Fluid Dynamics*, Vol. (submitted), 2020.

[24] Dhawan, S., and Narasimha, R., "Some Properties of Boundary-Layer Flow During Transition from Laminar to Turbulent Motion," *Journal of Fluid Mechanics*, Vol. 3, 1958, pp. 414–436.

[25] Fu, S., and Wang, L., "RANS Modeling of High-Speed Aerodynamic Flow Transition with Consideration of Stability Theory," *Progress in Aerospace Sciences*, Vol. 58, 2013, pp. 36–59.

[26] Zhou, L., Yan, C., Hao, Z., and Du, R., "Improved $k-\omega-\gamma$ Model for Hypersonic Boundary Layer Transition Prediction," *International Journal of Heat and Mass Transfer*, Vol. 94, 2016, pp. 380–389. doi:10.1016/j.ijheatmasstransfer.2015.11.048.

[27] Zhou, L., Li, R., Hao, Z., Zripov, D., and Yan, C., "Improved $k-\omega-\gamma$ Model for Crossflow-Induced Teransition Prediction in Hypersonic Flow," *International Journal of Heat and Mass Transfer*, Vol. 115, 2017, pp. 115–130. doi: 10.1016/j.ijheatmasstransfer.2017.08.013.

[28] Hao, Z., Yan, C., Qin, Y., and Zhou, L., "Improved $\gamma - Re_{\theta t}$ Model for Heat Transfer Prediction Hypersonic Boundary Layer Transition," *International Journal of Heat and Mass Transfer*, Vol. 107, 2017, pp. 329–338. doi:10.1016/j.ijheatmasstransfer. 2016.11.052.

[29] Qin, Y., Yan, C., Hao, Z., and Zhou, L., "A Laminar Kinetic Energy Transition Model Appropriate for Hypersonic Flow Heat Transfer," *International Journal of Heat and Mass Transfer*, Vol. 107, 2017, pp. 1054–1064. doi:10.1016/j.ijheatmasstransfer. 2016.11.012.

[30] Qin, Y., Yan, C., Hao, H., and Wang, J., "An Intermittency Factor Weighted Laminar Kinetic Energy Transition Model for Heat Transfer Overshoot Prediction," *International Journal of Heat and Mass Transfer*, Vol. 117, 2018, pp. 1115–1124. doi:10.1016/j.ijheatmasstransfer.2017.10.081.

[31] Bridges, T. J., and Morris, P. J., "Differential Eigenvalue Problems in Which the Parameter Appears Nonlinearly," *J. Comp. Phys.*, Vol. 55, No. 3, 1984, pp. 437–460.

[32] Paredes, P., "Advances in Global Instability Computations: from Incompressible to Hypersonic Flow," Ph.D. thesis, Universidad Politécnica de Madrid, 2014.

[33] Canuto, C., Hussaini, M. Y., Quarteroni, A., and Zang, T. A., *Spectral methods in fluid dynamics*, Springer, 1987.

[34] Wu, J., Yin, X., and Xiao, H., "Seeing Permeability from Images: Fast Prediction with Convolutional Neural Networks," *Science Bulletin*, Vol. 63, No. 18, 2018, pp. 1215–1222. doi:10.1016/j.scib.2018.08.006.

[35] Litton, D., Edwards, J., and White, J., "Algorithmic Enhancements to the VULCAN Navier-Stokes Solver," AIAA Paper 2003-3979, 2003. doi:10.2514/6.2003-3979.

[36] Kimmel, R., Adamczak, D., Paull, A., Paull, R., Shannon, J., Pietsch, R., Frost, M., and Alesi, H., "HIFiRE-1 Ascent-Phase Boundary-Layer Transition," *Journal of Spacecraft Rockets*, Vol. 52, No. 1, 2015, pp. 217–230.

[37] Kimmel, R., Adamczak, D., Gaitonde, D., Rougeux, A., and Haynes, J., "HIFiRE-1 Boundary Layer Transition Experiment Design," AIAA Paper 2007-0534, 2007.

[38] Rumsey, C., Biedron, R., and Thomas, J., "CFL3D: Its History and Some Recent Applications," NASA TM-112861, 1997.